Effect of temperature on carbon nanotube diameter and bundle arrangement: Microscopic and macroscopic analysis

I. Hinkov
LIMHP, Université Paris 13, Avenue J. B. Clément, 93430 Villetaneuse, France

J. Grand and M. Lamy de la Chapelle
LNIO, Université de Technologie de Troyes, 12 rue Marie Curie, BP2060, 10010 Troyes cedex, France

S. Farhat[a)]
LIMHP, Université Paris 13, Avenue J. B. Clément, 93430 Villetaneuse, France

C. D. Scott
NASA, Lyndon B. Johnson, Space Center ES4, Houston, Texas 77058

P. Nikolaev
G. B. Tech/NASA, Johnson, Space Center, Houston, Texas 77258

V. Pichot and P. Launois
Laboratoire de Physique des Solides (UMR CNRS 8502), bât. 510, Université Paris Sud, 91405 Orsay cédex, France

J. Y. Mevellec and S. Lefrant
LPC, Institut des Matériaux de Nantes, Université de Nantes, BP 32229, 44322 Nantes cedex, France

(Received 29 July 2003; accepted 10 November 2003)

The diameter distribution of the nanotubes produced by electric-arc discharge are measured using Raman spectroscopy at various wavelengths. These measurements agree with the results provided by two other techniques: high-resolution transmission electron microscopy and x-ray diffraction. The mean tube diameter shifts more than 0.1 nm with the increase of argon in the inert atmosphere. Some argon concentrations favored the synthesis of metallic tubes with specific diameters. Furthermore, the background gas influences the macroscopic characteristics of nanotube yield and bundle size, as determined by Brunauer–Emmett–Teller surface area measurements and x-ray diffraction. The information collected on nanotube diameter and arrangement is correlated with temperatures calculated using a numerical model of the plasma generated between the two electrodes. Indeed, plasma temperature control during the production process is achieved using argon–helium mixtures as buffer gases. The variation of the gas mixture from pure argon to pure helium changes the plasma temperature and hence the nanotube diameter. © *2004 American Institute of Physics.* [DOI: 10.1063/1.1638620]

I. INTRODUCTION

The diameter of single-wall carbon nanotubes (SWCNTs) is an important property and is of interest for new applications that rely on diameter uniformity or the unique chemical properties of certain types. Understanding the factors that affect the diameter may lead to a better understanding of the growth mechanism of the nanotubes. This work focuses on diameter control of SWCNTs during the electric-arc discharge process. However, to control the nanotube diameter, arc parameters must be controlled carefully. Due to the large variety in process parameters, much trial and error goes into optimizing growth conditions. In our previous work,[1] we controlled the average nanotube diameter using different gas mixtures in the arc reactor. In this study, we bring additional evidence about the efficiency of this method by microscopic [high-resolution transmission electron microscopy (HRTEM) and Raman spectroscopy] and macroscopic [Brunauer–Emmett–Teller (BET), x-ray diffraction] analysis of the nanotubes. Understanding the process parameters involved is aided by numerical modeling of the heat transfer in the arc. Characterization of nanotubes using various techniques gives fundamental information, specific for each technique, on the influence of the inert gas on the nanotube diameter. A Raman spectrum of SWCNTs is generally divided into two parts. The first one corresponds to the ''Radial Breathing Modes'' where the frequency of vibration depends directly on the diameter of the SWCNTs. The second one concerns the tangential modes that give insight into the electronic properties of the SWCNTs. The results obtained by Raman spectroscopy are complemented by HRTEM analysis. A statistical analysis of HRTEM pictures gives additional information on the diameter distribution. Macroscopic characteristics of nanotubes, such as BET surface area of as produced nanotubes and x-ray diffraction, show an important and reproducible effect of the inert gas on the morphology of the material (yield of nanotubes and number of

a)Author to whom correspondence should be addressed; electronic mail: farhat@limhp.univ-paris13.fr

nanotubes per bundle). Finally, mathematical modeling of the process can help understanding the effect of the buffer gas on the temperature distribution in the reactor. A one-dimensional mathematical model is developed that solves for the velocities, temperature and concentration of species in the inter-electrode gap for specific conditions of nanotube growth. In order to understand the experimental results, a comparison is made of temperature profiles obtained with argon, helium and their mixtures.

II. EXPERIMENT

Single-wall nanotube samples are obtained by the electric-arc discharge method between carbon electrodes, described in detail earlier.[1] The process consists of evaporation (in a buffer gas) of graphite anodes with a drilled hole and packed with a mixture of graphite, nickel and yttrium. The final molar ratio of C/Ni/Y including the outer graphite shell was 94.8:4.2:1. The run was made with a direct current of 100 A, and yielded 20 V for pure argon to 40 V for helium, for an inter-electrode gap of 3 mm. Mixtures of argon and helium are used as buffer gases. The percentage of argon was varied from 0% to 100% in steps of 20%. Finally, the total pressure of the mixture was fitted as a function of argon percentage by a linear interpolation between 100 and 660 mbar. These pressures for pure gases were found by Journet[2] to insure optimum nanotube yield. For nickel/yttrium catalyst and the fairly narrow range of pressures she reported, the variation in nanotube diameter was not large.[1,2] However, Saito, Tani, and Kasuya[3] have shown for Rh/Pt catalysts in the arc process a fairly strong dependence of the diameter of SWNTs on pressure over the range of 50–1520 Torr. They attribute this to the effect of pressure on process temperatures. As our synthesis setup is similar to the one used by Journet, we assume that the pressure has little influence on tube diameters, and, therefore, it is not the main parameter to be considered.

To characterize the synthesized nanotubes, we also choose to perform some resonant Raman studies. As reported in the literature,[4–7] it is necessary to use several excitation wavelengths to excite various diameter and chirality tubes. In our case, we used the following laser lines: 514.5 nm (argon laser), 632.8 nm (He–Ne laser), 676.4 nm (krypton laser) and 1064 nm [Nd:yttrium–aluminum–garnet (YAG) laser]. Raman spectra were recorded at room temperature and different spectrophotometers were used: a Jobin-Yvon T64000 triple monochromator spectrophotometer with argon and krypton lasers, a Jobin-Yvon Labram with He–Ne laser and a Brüker FT Raman RFS 100 with Nd:YAG laser. For all spectra, the spectral resolution was about 1 cm^{-1}, and by taking advantage of the confocal microscope of the T64000 and Labram spectrometers, spatial resolution was close to 1 μm.

Transmission electron microscopy (TEM) samples are prepared in a somewhat unusual fashion. A tiny piece of dry nanotubes is placed on the dry TEM grid, followed by a droplet of methanol. The nanotube samples become flattened and stick to the grid as the methanol dries; and in many places nanoropes form loops. When such loops are parallel to the electron beam of TEM, one can see little circles, which are cross sectional images of nanotubes. We have used a program, which allows fitting circles onto the cross sectional images, to measure their diameters. We consider such measurements more precise than measurements on the in-plane nanotubes. Images are scanned at 1200 dpi; TEM magnification factor is 23 nm/cm at 500kX magnification.

In addition to Raman spectroscopy and electron microscopy, we characterize the materials at a macroscopic level. The BET surface area[8] of the single-wall carbon nanotube samples is determined by nitrogen adsorption at 77 K, using a BET COULTER SA 3100 instrument. Prior to absorption, the samples were degassed at 393 K for at least a 1/2 h. We determine the dead volume by introducing helium gas. A constant flow of nitrogen gas was adsorbed at 77 K and the pressure recorded. The adsorption process on a surface can be described by the BET equation.

The x-ray scattering experiments have been performed on a rotating anode. Cu $K\alpha$ radiation ($\lambda = 1.5418$ A) was selected by reflection on a doubly bent graphite monochromator. The powder samples were sealed in 1-mm-diam glass capillaries and placed in an evacuated x-ray chamber to remove air scattering. Diffraction patterns were measured on a cylindrical ($\varphi = 114.6$ mm) imaging plate. The profiles reported in this article are recorded along the equatorial line of the imaging plate (Debye–Scherrer geometry). Intensities are corrected for polarization effects, and a broad diffuse scattering signal around 1.8 $Å^{-1}$, coming from the glass capillary, has been subtracted from the x-ray scattering profiles. The volume of the samples studied is about 1 mm^3.

III. RESULTS

A. Raman spectroscopy

Raman spectroscopy turns out to be a powerful and nondestructive tool to characterize single-wall carbon nanotubes (SWNTs), since some vibrational modes are related to some of their structural features.[4–7,9] The diameter (d), for example, can be assessed by measuring the radial breathing mode (RBM) frequency and applying the formula[7]

$$\nu_{\mathrm{RBM}}\ (\mathrm{cm}^{-1}) = \frac{223.75}{d\ (\mathrm{nm})}. \tag{1}$$

Another formula has been proposed[10] to estimate the diameter of isolated SWNTs

$$\nu_{\mathrm{RBM}}\ (\mathrm{cm}^{-1}) = \frac{248}{d\ (\mathrm{nm})}. \tag{2}$$

Neither formula takes into account the Van der Waals interaction between tubes when they are arranged in bundles. This interaction does influence the breathing vibration of individual tubes. This was calculated by different groups,[11,12] and also by Buisson *et al.*,[13] who predict an up shift between 10 and 20 cm^{-1}, depending on the size of the bundle. This effect is difficult to demonstrate experimentally since the samples may contain, in general, both isolated tubes and bundles. Nevertheless, it appears that chemically induced dispersion can lead to the preparation of large concentrations of isolated tubes as observed in atomic force microscopy. This was achieved by Marcoux *et al.*[14] applying fluorination/

TABLE I. Resonant diameter and electronic character (M: metallic, SC: semiconducting) for each wavelength used in Raman experiments.

Wavelength (nm)	514.5	632.8	676.4	1064
Resonant diameter (nm)	1.32	1.15	1.45	1.35
Electronic character	SC	M	M	SC

defluorination chemical procedures. In this case, it is observed that two bands in the RBM region can be associated with tubes in bundles and isolated tubes, respectively.

It would be speculative to apply any type of correction in the RBM frequencies since our samples consist of bundles of different sizes and of isolated tubes. The use of either formula (1) or (2) slightly shifts the diameter distribution, but does not modify the observed trend. Therefore, we used formula (1) to estimate in relative values of the nanotube diameter distribution in our samples.

In resonant Raman experiments, using different excitation laser lines allowed us to distinguish between types of SWNTs. This arises from the fact that the electronic density of states of SWNTs exhibit van Hove singularities, which energy positions are strongly dependent on the nanotube diameter (inversely proportional) and on the metallic (M) or semiconductor (SC) nature.[15] Some electronic transitions are easily induced between van Hove singularities, allowing a selective characterization of SWNTs.[4] These nanotubes are listed in Table I.

For each wavelength, from 5 to 10 spectra were recorded at different locations in the sample, providing average data on nanotube characteristics assumed to represent the whole sample. The radial breathing mode is fitted with Lorentzian lines the positions and areas of which provide the SWNT diameters and relative concentrations, respectively (Fig. 1). Therefore, for each sample and wavelength, we deduce the diameter distribution and calculate an average diameter.

In Fig. 2, the average diameter is shown as a function of argon percentage in the inert atmosphere used during the SWNT production. For the three wavelengths: 514.5, 632.8, and 676.4 nm, we clearly notice a continuous decrease of the diameter with increasing Ar percentage. The biggest diameter (1.4 nm) is obtained with 20% of Ar, whereas 80% and 100% of Ar yield the smallest diameter, close to 1.3 nm.

Thus, changing the gas mixture appears to induce a 0.1 nm variation in the SWNT diameter. This trend is confirmed by a shift in the diameter distribution shown in Fig. 3 for 514.5 and 676.4 nm. As the Ar percentage increases, the concentration of largest diameters (1.35–1.5 nm) decreases while the concentration of smallest ones (1.1–1.2 nm) increases. One can even notice that some very small nanotubes (0.8–1 nm) are produced at a high Ar percentage.

For the 1064 nm excitation wavelength (i.e., 1.16 eV), the SWNT diameter appears to be nearly constant for all Ar percentage. Unlike other wavelengths, the excitation energy (1.16 eV) matches exactly the first electronic transition allowed by van Hove singularities. Hence, there is a strong resonant effect with SWNTs of 1.35 nm in diameter. The RBM band assigned to this resonant diameter is much more intense than all the others. Therefore, any changes in the

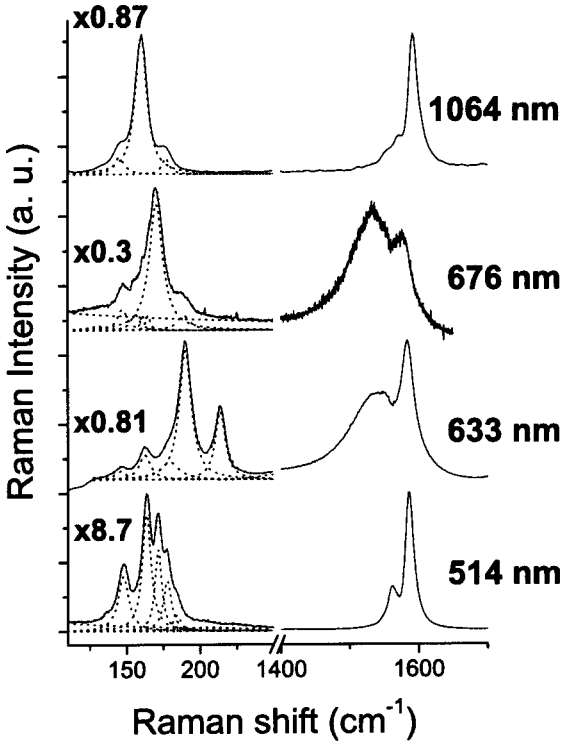

FIG. 1. Relevant Raman spectra recorded on the 0% of Ar sample for four laser excitation wavelengths.

relative intensities of other RBM bands (i.e., other diameters) will not affect the computed average diameter very much. Still, some very small variations, ranging from 1.39 nm for 80% of Ar to 1.41 nm for 40% of Ar, can be seen.

Raman spectra recorded at 632.8 and 676.4 nm exhibit a Breit–Wigner–Fano line shape at 1540 cm^{-1} which is related to the resonance of metallic SWNTs (Fig. 1).[16] The relative intensity of the RBM bands assigned to diameters 1.15 and 1.3 nm (according to Table I, are in resonance for 632.8 and 676.4 nm, respectively) is always higher than for other diameters (Fig. 3). Because of resonant behavior of tubes of these diameters, they are assumed metallic. The evolution of the concentration of these resonant diameters with the Ar percentage (Fig. 4) is nearly constant except for 80% and 100% of Ar. It means that for these two percentages, the concentration of metallic tubes increases. Therefore, for an

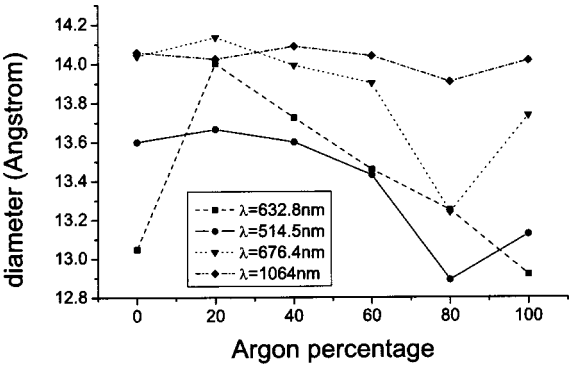

FIG. 2. Variation of the average tube diameter with the argon percentage.

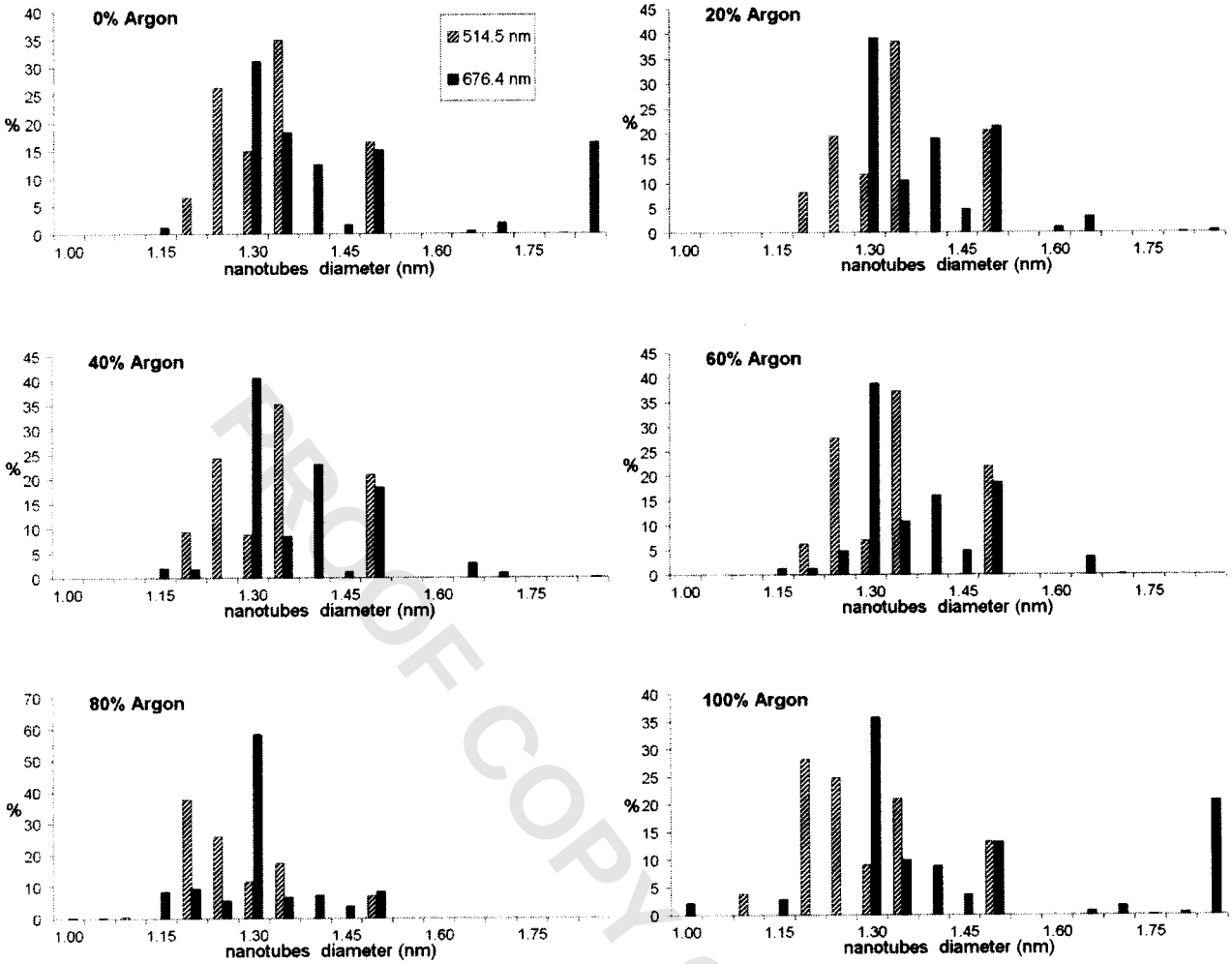

FIG. 3. Nanotube diameter distribution from Raman spectra at 514.5 and 676.4 nm wavelength excitation.

appropriate percentage of Ar, the production of metallic tubes with a specific diameter is favored.

Figure 3 also shows a specific behavior for 20% and 80% of Ar since these percentages, respectively, exhibit the biggest and the smallest diameters. Adding a small amount of another gas to a pure atmosphere seems to induce a step in the diameter distribution.

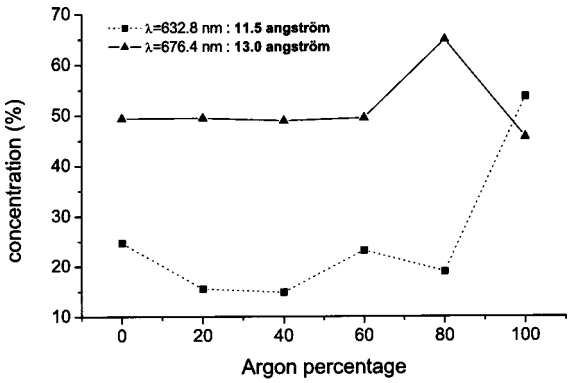

FIG. 4. Variation of metallic tube concentration vs argon percentage obtained from Raman spectra excited at 632.8 and 676.4 nm wavelengths.

B. TEM observations

Figure 5 shows HRTEM for nanotubes synthesized under different atmospheres. Nanotube yield is good for 0% Ar and 20% Ar, a little less in 40% Ar, and then decreases significantly in 60% Ar and 80% Ar. For Ar concentrations from 0% to 80%, the tube diameters were measured. For each sample, several nanotubes have been counted as followed: 0%—116 tubes, 20%—115 tubes, 40%—99 tubes, 60%—34 tubes, 80%—19 tubes. These numbers actually reflect very well on the abundance of nanotubes in each sample. For 100% argon, the number of nanotubes is extremely low. However, a few tubes can be seen, but their orientations were not suitable for measuring diameters. The diameter distributions are reported in Fig. 6, where they are fitted with Gaussian curves. For each sample, X_c is the center of the distribution (which is the most accurate measure of the mean diameter), and W is the distribution full width (not half-width). This indicates a clear decrease of the tube diameter with argon percentage. Moreover, the diameter distribution measured is very close to the one observed by Raman spectroscopy at 514.5 nm (Fig. 3) with the same diameters and the same trend when we change the argon concentration.

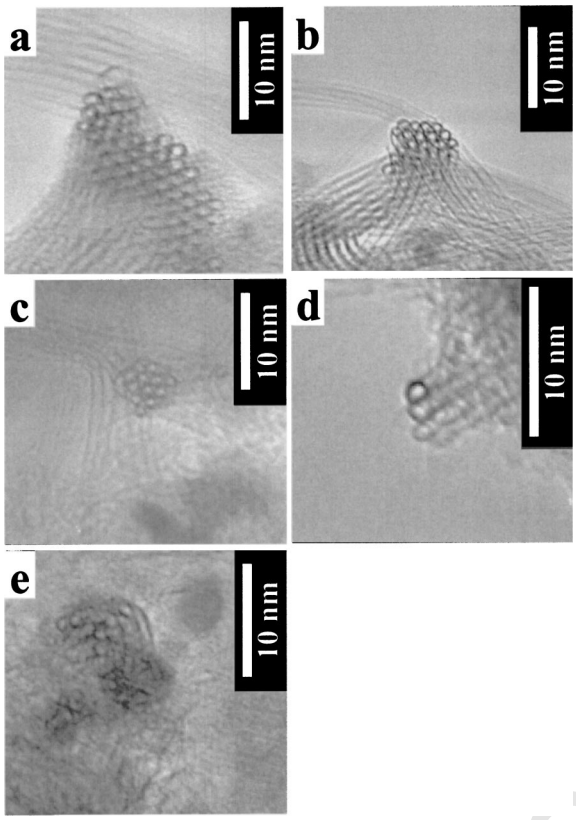

FIG. 5. HRTEM images of the samples: (a) pure helium, (b) 20% argon, (c) 40% argon, (d) 60% argon, and (e) 80% argon.

C. X-ray scattering

To get further information on the tube diameter and bundle arrangement, we have performed some x-ray scattering experiments for all argon percentages. Figure 7 shows an x-ray scattering profile obtained for nanotubes synthesized under a pure He atmosphere. The peak around 0.47 Å^{-1} is the (1,0) peak of nanotubes organized in bundles on a two-dimensional hexagonal lattice.[17,18] Weaker intensity peaks corresponding to wave vectors $Q \approx 0.77$, 0.9, and 1.16 Å^{-1} are indexed as (1,1), (2,0) and (2,1) peaks, respectively. The one at 1.57 Å^{-1} corresponds to the overlapping of the (2,2) and (3,1) peaks. The peak positions and widths depend on the nanotube diameters and on the bundle sizes. The data have been fitted as a function of the mean nanotube diameter φ_m; the full width at half maximum w of the distribution of the nanotube diameters in different bundles, taken as Gaussian; and on the number of tubes in the bundles. The theoretical calculated intensity[19] is

$$I_{\text{calc}}(Q) \propto \frac{f_c(Q)^2}{Q} \int p(\Phi) J_0(Q\Phi/2)^2 \sum_{i,j} J_0(QR_{ij}) d\Phi, \tag{3}$$

where f_c is the x-ray form factor of carbon, J_0 is the zero-order Bessel function, Φ is the nanotube diameter in a bundle, R_{ij} is the distance between the centers of two nanotubes in the same bundle (in a plane perpendicular to the nanotube axis), and $p(\Phi)$ is the distribution of nanotube diameters among different bundles. The fitting procedure compares the calculated intensities, convoluted with the instrument function (taken as a Gaussian with full width at half maximum of 0.04 Å^{-1}), with the measurements. One finds: $\Phi \approx 1.3$ nm and $w \approx 0.1$ nm for bundles of about 40 nanotubes (the bundle diameter is ≈ 10 nm), which agree with the HR-TEM and Raman results. The calculated curve is compared with the measurements in Fig. 7.

Several samples corresponding, respectively, to 0%, 20%, 40%, 60%, 80% and 100% Ar atmospheres were studied. Different x-ray scattering profiles can be obtained for different samples synthesized under the same conditions. This is due to differences in nanotube diameters or bundle sizes. As the samples were presumably taken from different parts of the collaret on the cathode, these differences are attributed to gradients of temperature around the cathode, as demonstrated by one-dimensional calculations of the heat transfer between the cathode and anode (see below). All the results are summarized in Table II, and some of them are drawn in the inset of Fig. 7. The following tendency can be deduced from the experiments. When the amount of argon is increased, the (1,0) peak becomes much weaker or disappears. This peak corresponds to relatively large bundles of about 10 nm in diameter for 0% Ar atmosphere. Its intensity should decrease for a smaller yield of nanotubes, or if the nanotubes are assembled in small bundles. In this latter case, the peak width increases so that it becomes undistinguishable from background. Our results are thus in agreement with BET (see below) and TEM measurements which point toward a decrease in the nanotube yield and in the bundle sizes with increasing Ar gas concentrations. Moreover, with increasing Ar gas concentration, an increase of the (1,0) peak position (when this peak is observed) can be deduced from the data. Typically, it moves from 0.47 Å^{-1} to 0.49 Å^{-1} for 0% and 100% Ar atmosphere. These positions correspond to mean tube diameters of about 1.3 and 1.2 nm, respectively. The average tube diameter decreases by 0.1 nm as the inert gas changes from 0% Ar to 100% Ar, as also observed with HRTEM and Raman spectroscopy. Although one should keep in mind that only nanotubes assembled in sufficiently large bundles contribute to the signal, the agreement with the TEM and Raman results can be emphasized.

D. BET surface area

In Fig. 8, we report the variation of the BET surface area of the samples with the argon mole fraction in the background gas, and the corresponding isotherms of nitrogen adsorption. The isotherms are of type II of the IUPAC classification. The surface area varied from 200 to 450 $\text{m}^2\,\text{g}^{-1}$, where the maximum value of 440 $\text{m}^2\,\text{g}^{-1}$ is found for 20% argon, and decreases with increasing the argon percentage. The nitrogen in the BET measurements does not access significant surface area in the space between nanotubes in a bundle.[20] The nanotube ends are closed and the BET surface area is attributed to the outer surface of a SWCNTs organized in bundles.[18] The measured values are about an order of magnitude lower than for the calculated area of single nanotubes (1300 $\text{m}^2\,\text{g}^{-1}$).[21] Peigney *et al.*[22] have demonstrated that the specific area of bundles of nanotubes depends only on the number of involved SWCNTs. The surface area

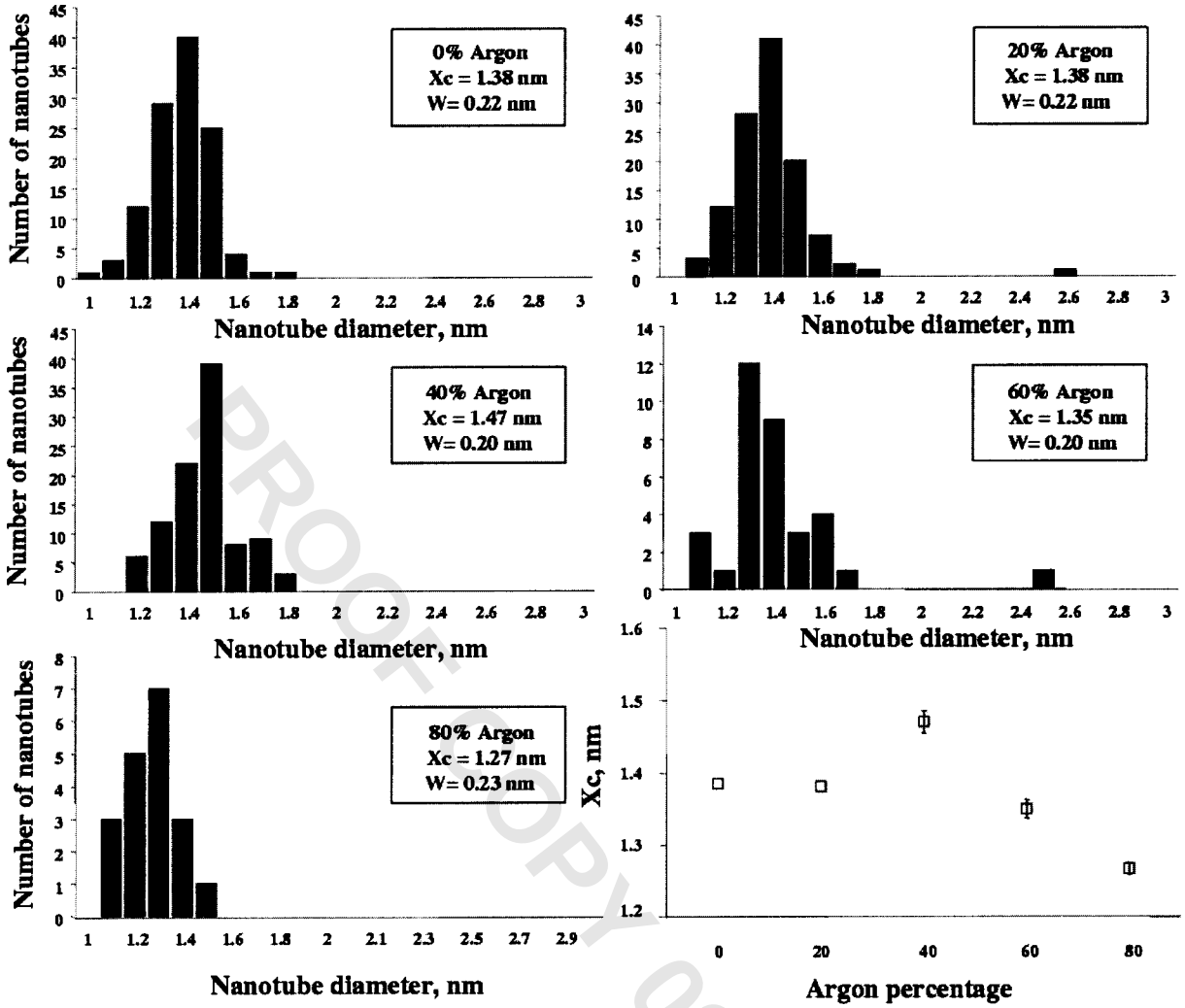

FIG. 6. Diameter distribution of SWNT measured from TEM pictures. X_c is the center of the distribution and w is the distribution full width. On the bottom roght, X_c is plotted vs the argon concentration and W is plotted as an error bar.

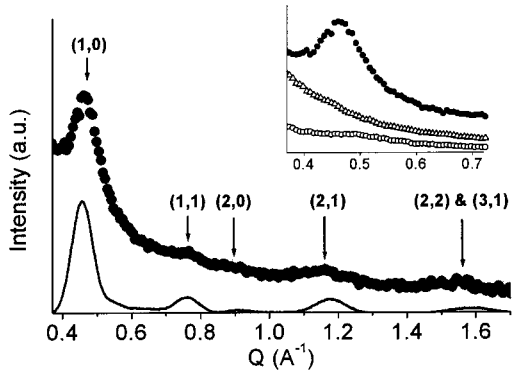

FIG. 7. X-ray scattering study of nanotubes synthesized under 0% Ar atmosphere. Solid circles: measurements, continuous line: calculated spectrum (after convolution by resolution). The nanotubes are organized in bundles, in a two-dimensional hexagonal lattice: peaks are indexed within basis of the corresponding reciprocal lattice. X-ray scattering profiles for nanotubes synthesized under different helium–argon atmospheres are reported in the inset. Solid circles: 0%Ar atmosphere [strong (1,0) peak], open triangles: 60% Ar atmosphere [no (1,0) peak observed] and open circles: 100% Ar atmosphere [weak (1,0) peak observed]. The intensities have been arbitrarily translated for the sake of clarity.

of bundles is equal to the surface area of single nanotube multiplied by a correction factor. This factor decreases as the number of SWCNTs in the bundle increases. In addition, the specific surface area of isolated nanotubes does not depend on their diameter, since the tubes are of the same wall thickness. The HRTEM images of our samples showed that the number of SWCNTs in the ropes decreases as the percentage of argon in the inert gas increases. Thus, we had hoped for an increase in the BET surface area as the argon percentage was increased. Therefore, it appears that the observed decrease in the BET surface area must result from a lower abundance of SWNTs in the samples. Therefore, the BET surface area measurement seems to predict a qualitative trend in the yield of nanotubes in the samples: the lower the surface area, the lower the nanotube yield.

E. Modeling heat transfer

In order to analyze the effect of the buffer gas composition on the temperature profiles, a mathematical model was formulated under specific conditions of nanotube growth in the arc. The model cannot be considered of high fidelity to the detailed process. It is used to obtain trends of operating

TABLE II. Summary of the x-ray scattering study.

	0%Ar	20%Ar	40%Ar	60%Ar	80%Ar	100%Ar
Number of samples studied	6	2	3	3	2	6
Number of samples for which no (1,0) peak was observed	0	1	3	3	1	3
Position of the (1,0) peak when observed (angstrom^{-1})	0.42, 0.45, 0.45, 0.47, 0.47, 0.47	0.48	⋯	⋯	0.49	0.44, 0.49, 0.49

conditions as parameters, such as total power, gas composition and geometry, which are varied. This model is solved using the SPIN computer code developed by Kee *et al.*[23] This program computes species, temperature and velocity profiles in a steady-state one-dimensional stagnation-point flow, and incorporates temperature dependant fluid properties. The model is a boundary value problem consisting of a set of ordinary differential equations, solved by a finite difference procedure. We assume local thermal equilibrium (LTE) and solve the steady-state axial and radial momentum, species and energy equations in spatial one dimension between the anode and the cathode. The model accounts for carbon deposition at the cathode by a set of surface reactions that simulates nanotube growth. The steady-state assumption is justified because of the continuous adjustment of the interelectrode gap leading to a constant erosion of the anode, hence a constant condensation of carbon vapor close to the cathode. Local thermodynamic equilibrium was assumed based on the Bilodeau, Pousse, and Gleizes[24] model for fullerene synthesis by arc discharge in the same range of pressure as nanotube synthesis. The model equations are described in detail in Farhat, Hinkov, and Scott.[25] We will focus our discussion here on the thermal effect due to changing the buffer gas composition and its effect on the source and loss terms in energy balance equation. Source term q with the parameters set in Table III is determined from the arc current and voltage and surface radiation exchange between the cathode and the anode and the chamber. It accounts for the total input power integrated over its full spatial extent less surface radiative losses. The radiative losses Q_{rad} account for the net loss of energy by gas radiation. As indicated by Ioffe *et al.*,[26] Owano[27] and Murphy,[28] radiative losses are important when argon is used. In our model, the nonequilibrium radiation loss term Q_{rad} was estimated from Owano[27] using

$$Q_{\text{rad}} = 1.065 \times 10^{14} \alpha \exp\left(\frac{-141170}{T}\right)\left(\frac{W}{m^3}\right), \tag{4}$$

where α is a nonequilibrium factor [$\alpha=1$ for local thermal equilibrium (LTE) model and $\alpha=10$ for partial local thermal equilibrium (PLTE) model]. For each condition of Table III, we solve the model equations assuming three conditions for gas radiation: no radiation, LTE and PLTE. For all cases, the interelectrode gap was maintained at 3 mm and the current was set at 100 A. The temperature of the cathode is predicted as a part of the solution by the model and is plotted versus argon percentage in Fig. 9. From this figure, we can notice the strong effect of the radiative model (PLTE and LTE) on cathode temperature for high argon percentages. But, whatever the radiative model used, the cathode temperature decreases with argon. The calculated temperature gradient at the cathode versus percentage of argon in buffer gas is plotted in Fig. 10 and confirms the sensitivity of the solution on the buffer gas composition. The trend of the gradient is opposite the cathode temperature because the thermal conductivity of helium is much greater than argon.

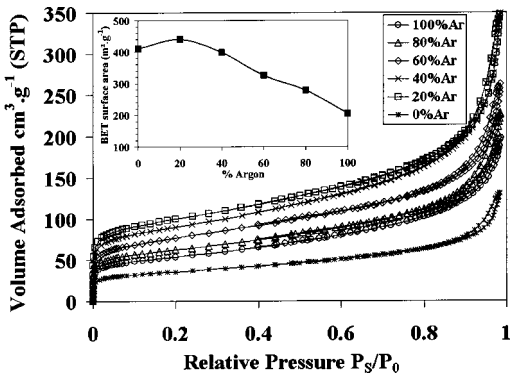

FIG. 8. Volume adsorption curves vs pressure for various argon concentrations. Inset: evolution of the BET surface with the argon concentration.

IV. DISCUSSION

According to the results presented herein (Raman spectroscopy, TEM, x-ray diffraction), two main conclusions on the effect of the composition of the inert atmosphere on nanotube structures arise. As the argon percentage increases, the diameter of the tubes decreases. Likewise, the number of tubes in the bundles and in the soot decreases. We assume that these effects are strongly related to the temperature and

TABLE III. Parameters of the simulation.

Percentage of argon in buffer gas	Pressure (mbar)	q (10^7 W m^{-2})
0	660	1.24
20	550	1.00
40	435	0.97
60	325	0.70
80	210	0.63
100	100	0.65

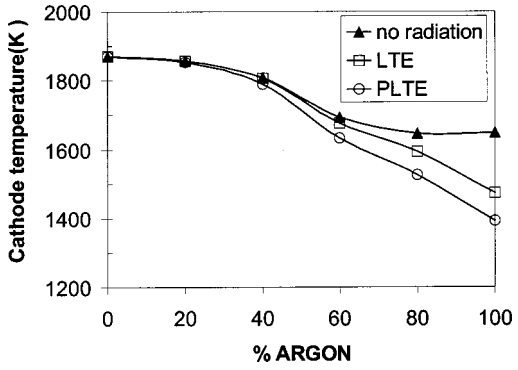

FIG. 9. Calculated cathode temperature vs buffer gas composition with no radiation, LTE radiation or PLTE radiation.

its gradient near the cathode, as will be shown. The interplay between the temperature and tube formation has already been reported by several authors. Actually, Bandow *et al.*[7] have shown that increasing the oven temperature during the laser ablation of catalyst—graphite target favored the production of nanotubes with larger diameters. Since then, other groups have also related the tube synthesis to the eutectic temperature of a carbon—catalyst phase.[29–31] They showed that nanotubes might be formed during a liquid–solid phase transition of the catalysts at a temperature ranging from 1300 to 1800 K depending on which catalysts are mixed with the carbon. Thus, nanotubes are created within a very narrow window of temperatures (values and gradient) that can be used to control the nanotubes structure. To regulate the temperature, several parameters can be varied, such as the target composition[32,33] and its temperature,[31] the inert atmosphere gas,[1,2,34,35] and for laser ablation production, the gas flow rate.[31] The results of all these experiments on the tube production show the great importance of the temperature and its gradient inside the synthesis chamber. Moreover, these effects concern not only the production rate but also the tube diameter as it increases when the chamber wall or the target temperature increases.[10,29,31]

Our results in the arc process confirm all the observations reported above for the laser ablation process. All the information collected about the nanotube structure and its arrangement is correlated with a model of the plasma generated between the two electrodes. We have seen clear evidence of the effect of temperature.

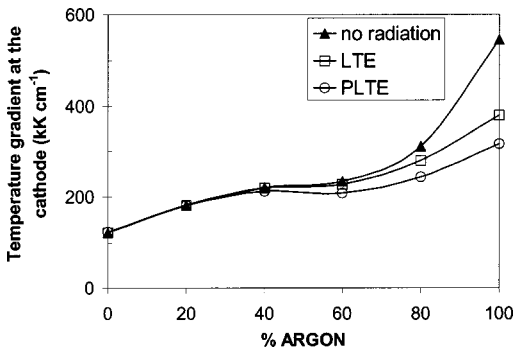

FIG. 10. Calculated temperature gradient close to the cathode vs buffer gas composition with no radiation, LTE radiation or PLTE radiation.

As mentioned previously, the nanotubes are created between 1300 and 1800 K.[29,30] Such temperatures are reached very close to the cathode (few micrometers). Elsewhere the temperature is above 2500 K. The cathode temperature and the gradient of temperature in the gas close to the cathode are then the main parameters to be considered. Changing the atmosphere composition, from pure helium to pure argon, entails a decrease of the cathode temperature greater than 200 K. This decrease is significant between 20% and 80%; and it induces a drop in the tube diameter as confirmed by all experimental techniques. The profile of the curve in Fig. 9 for an argon concentration less than 20% (and greater than 80% in no radiation case) shows very small variation compared to the other concentrations. This can explain the peculiar variation of the average tube diameter.

If the tube diameters are smaller, we can assume that the surface of interaction between two tubes is also smaller. This entails weaker Van der Waals interaction between the adjacent tubes. It is then energetically less favorable for the tubes to be packed together in a bundle arrangement when their diameter decreases. Since the diameter decreases with the increase of argon concentration, fewer tubes are observed in the bundles at higher argon concentration. As the temperature gradient increases with the argon percentage, the window of temperatures suitable for tube formation is then reduced. The extent of the production volume is also reduced and this decreases the number of tubes synthesized. Thus, the decrease in the production rate, observed by BET and HR-TEM, is attributed to a higher gradient of temperatures.

V. CONCLUSION

To summarize, we varied the inert atmosphere composition in electric-arc discharge process to control the temperature inside the production chamber, thereby affecting the diameter distribution of the nanotubes. It was also observed that the nanotube production rate and the size of bundles decrease with an increase of the argon percentage. Moreover, from the results of modeling the arc discharge plasma and from all experimental data, we give evidence of the close relation between the temperature inside the production chamber and the synthesis of the nanotubes. We then conclude that a fine control of the temperature allows one to control tube structures, such as diameter or bundle arrangement. It is also of real importance to control the temperature gradient to improve the production rate.

ACKNOWLEDGMENTS

V. Pichot and P. Launois acknowledge helpful discussions with R. Almayrac and N. Bendiab.

[1] S. Farhat, M. Lamy de La Chapelle, A. Loiseau, C. Scott, S. Lefrant, C. Journet, and P. Bernier, J. Chem. Phys. **115**, 10 (2001).
[2] C. Journet, Ph.D. thesis, Académie de Montpellier, Université de Montpellier II, 1998.
[3] Y. Saito, Y. Tani, and A. Kasuya, J. Phys. Chem. B **104**, 2495 (2000).
[4] A. Kasuya, Y. Sasaki, Y. Saito, K. Tohji, and Nishina, Phys. Rev. Lett. **78**, 4434 (1997).
[5] A. M. Rao, E. Richter, S. Bandow, B. Chase, P. Ek-lund, K. Williams, S. Fang, K. Subbaswamy, M. Menon, A. Thess *et al.*, Science **275**, 187 (1997).

[6] M. Lamy de la Chapelle, S. Lefrant, C. Journet, W. Maser, and P. Bernier, Carbon **36**, 705 (1998).
[7] S. Bandow, S. Asaka, Y. Saito, A. M. Rao, L. Grigorian, E. Richter, and P. C. Eklund, Phys. Rev. Lett. **80**, 3779 (1998).
[8] S. Brunauer, P. Emmett, and E. Teller, J. Am. Chem. Soc. **60**, 309 (1938).
[9] L. Alvarez, A. Righi, S. Rols, E. Anglaret, D. Laplaze, and J. Sauvajol, Chem. Phys. Lett. **316**, 186 (2000).
[10] A. Jorio, R. Saito, J. H. Hafner, C. M. Lieber, M. Hunter, T. M. Clure, G. Dresselhaus, and M. S. Dresselhaus, Phys. Rev. Lett. **86**, 1118 (2001).
[11] L. Henrard, E. Hernandez, P. Bernier, and A. Rubio, Phys. Rev. B **60**, R8521 (1999).
[12] D. Kahn and J.-P. Lu, Phys. Rev. B **60**, 6535 (1999).
[13] J. P. Buisson, O. Chauvet, S. Lefrant, C. Stephan, and J. M. Benoit, Proceedings of the Materials Research Society Fall Metting, 2001, p. 633 (unpublished).
[14] P. Marcoux, J. Schreiber, P. Batail, S. Lefrant, J. Renouard, G. Jacob, D. Albertini, and J. Y. Mevellec, J. Royal Soc. Chem, PCCP , (2002) (in press).
[15] C. T. White and J. W. Mintmire, Nature (London) **394**, 29 (1998).
[16] M. Pimenta, A. Marucci, S. Empedocles, M. Bawendi, E. Hanlon, A. Rao, P. Eklund, R. Smalley, G. Dresselhaus, and M. Dresselhaus, Phys. Rev. B **58**, R16016 (1998).
[17] C. Journet, W. K. Maser, P. Bernier, A. Loiseau, M. Lamy de la Chapelle, S. Lefrant, P. Deniard, R. Lee, and J. E. Fischer, Nature (London) **388**, 756 (1997).
[18] A. Thess, R. Lee, P. Nikolaev, H. J. Dai, P. Petit, J. Robert, C. H. Lee, S. G. Kim, A. G. Rinzler, and D. T. Colbert *et al.*, Science **273**, 483 (1996).
[19] S. Rols, R. Almairac, L. Henrard, E. Anglaret, and J.-L. Sauvajol, Eur. Phys. J. B **10**, 263 (1999).
[20] R. Baughman, C. Cui, A. Zakhidov, Z. Iqbal, J. Barisci, G. Spinks, G. Wallace, A. Mazzoldi, D. D. Rossi, and A. Rinzler *et al.*, Science **284**, 1340 (1999).
[21] Y. Ye, C. C. Ahn, C. Witham, B. Fultz, J. Liu, A. G. Rinzler, D. Colbert, K. A. Smith, and R. E. Smalley, Appl. Phys. Lett. **74**, 2307 (1999).
[22] A. Peigney, C. Laurent, E. Flahaut, R. Bacsa, and A. Rousset, Carbon **39**, 507 (2001).
[23] R. J. Kee, F. M. Rupley, J. A. Miller, M. E. Coltrin, J. F. Grcar, E. Meeks, H. K. Mo_at, A. E. Lutz, G. Dixon-Lewis, M. D. Smooke *et al.*, *CHEMKIN Collection* (Reaction Design, Inc., San Diego, CA, 2001), vol. Release 3.6.
[24] J. Bilodeau, J. Pousse, and A. Gleizes, Plasma Chem. Plasma Process. **18**, 285 (1998).
[25] S. Farhat, I. Hinkov, and C. D. Scott, J. Nanosci. Nanotechnol. Special Issue , (2003).
[26] I. Iofbe, V. Koss, N. Perelman, and D. Hilton, J. Phys. D **30**, 792 (1997).
[27] T. G. Owano, HTGL Rep. No. I-279, Stanford University, 1991.
[28] A. A. Murphy, J. Phys. D **31**, 3383 (1998).
[29] H. Kataura, Y. Kumazawa, Y. Maniwa, Y. Ohtsuka, R. Sen, S. Suzuki, and Y. Achiba, Carbon **38**, 1691 (2000).
[30] A. A. Puretzky, D. B. Geohegan, H. Schittenhelm, X. Fan, and M. A. Guillorn, Appl. Surf. Sci. **197–198**, 552 (2002).
[31] L. Alvarez, T. Guillard, J. L. Sauvajol, G. Flamant, and D. Laplaze, Chem. Phys. Lett. **342**, 7 (2001).
[32] W. K. Maser, E. Munoz, M. T. Martinez, A. M. Benito, and G. F. de la Fuente, Opt. Mater. **17**, 331 (2001).
[33] W. K. Maser, A. M. Benito, and M. T. Martinez, Carbon **40**, 1685 (2002).
[34] E. Munoz, W. K. Maser, A. M. Benito, G. F. de la Fuente, and M. T. Martinez, Synth. Met. **103**, 2490 (1999).
[35] E. Munoz, W. K. Maser, A. M. Benito, M. T. Martinez, G. F. de la Fuente, Y. Maniette, A. Righi, E. Anglaret, and J. L. Sauvajol, Carbon **38**, 1445 (2000).